Nuclear Instruments and Methods in Physics Research A 840 (2016) 186–191

Contents lists available at ScienceDirect

Nuclear Instruments and Methods in Physics Research A

journal homepage: www.elsevier.com/locate/nima

Pulse shape discrimination properties of $Gd_3Ga_3Al_2O_{12}$:Ce,B single crystal in comparison with CsI:Tl

S. Rawat[a,b], Mohit Tyagi[a,*], P.K. Netrakanti[c], V.K.S. Kashyap[c], A. Mitra[c], A.K. Singh[a], D.G. Desai[a], G. Anil Kumar[b], S.C. Gadkari[a]

[a] Technical Physics Division, Bhabha Atomic Research Centre, Mumbai 400085, India
[b] Department of Physics, Indian Institute of Technology, Roorkee 247667, India
[c] Nuclear Physics Division, Bhabha Atomic Research Centre, Mumbai 400085, India

ARTICLE INFO

Keywords:
Scintillator
Single crystal
Detector
Pulse shape discrimination

ABSTRACT

Single crystals of $Gd_3Ga_3Al_2O_{12}$:Ce,B and CsI:Tl were grown by Czochralski and Bridgman techniques, respectively. While both the crystals exhibited similar emission at about 550 nm, their scintillation decay times showed significantly different characteristics. The average scintillation decay time of $Gd_3Ga_3Al_2O_{12}$:Ce,B crystal was found to be about 284 ns for alpha excitation compared to 108 ns measured for a gamma source. On the other hand in CsI:Tl crystals, the alpha excitation resulted in a lower average decay time of 600 ns compared to 1200 ns with gamma excitation. Their pulse shape discrimination (PSD) for gamma and alpha radiations were studied by coupling the scintillators with photomultiplier tube or SiPM and employing an advanced digitizer as well as a conventional zero-crossing setup. In spite of having a poor α/γ light yield ratio, the PSD figure of merit and the difference of zero-crossing time in $Gd_3Ga_3Al_2O_{12}$:Ce,B crystals were found to be superior in comparison to CsI:Tl crystals.

1. Introduction

Among cerium doped oxide scintillators having garnet structure such as $Y_3Al_5O_{12}$ and $Lu_3Al_5O_{12}$ etc., gadolinium gallium aluminum garnet ($Gd_3Ga_3Al_2O_{12}$, also called GGAG) has shown the best combination of the scintillation characteristics [1–3]. It exhibits high density (6.7 g/cm^3), effective atomic number (55), high light yield (about 54,000 pH/MeV) and fast decay time (55 ns) [4,5]. The scintillation performance of GGAG:Ce in gamma spectroscopy has been extensively investigated by employing various photo-sensors [6]. However, its charged particle spectroscopy is yet to be explored in details. Moreover, the development of new photo sensors such as SiPM and the state-of-the-art electronics has led to an investigation of crystal's performance in charged particle identification in order to explore the possibility of using them in the applications requiring compact detector geometry.

The pulse shape discrimination (PSD) technique has been utilized in various crystals such as NaI:Tl [7], CsI:Tl [8], BaF_2 [9], ZnS:Ag [10], $LaBr_3$, $LaCl_3$ [11], YAG:Ce [12], LuAG:Ce [13] and GGAG:Ce [14] for the explicit identification of charged particles, gammas and neutrons. The scintillation decay curve for these crystals consists of more than one exponential component. The relative ratio of these components depends on the nature of the exciting radiation due to the difference in ionization density caused by different energy loss mechanisms. Subsequently, the shape of the decay pulse can be used to distinguish the exciting radiations. The PSD techniques have in past been extensively utilized in the neutron spectroscopy for discriminating the gamma background [15]. Also, fission events generating heavy charged particles can also be identified by using these techniques [16]. CsI(Tl) scintillator crystals have been widely used for the detection of charged particle owing to their excellent light output of about 66,000 pH/MeV, two decays of 680 and 3000 ns, emission at 550 nm and the cost effectiveness [17]. Due to the green-yellow emission, GGAG:Ce crystals can also be used with silicon based photo-sensors to fabricate the compact detectors in this regard [18]. The GGAG:Ce has an edge over CsI:Tl in being non-hygroscopic, denser and has a faster decay time. Boron codoping has been reported to improve the scintillation light yield further. The self-absorption of scintillation light output (LO) in the GGAG:Ce,B crystal also decreases which results in the improvement of energy resolution from 9% to 7.8% [5]. However, the PSD in boron codoped GGAG:Ce has not been studied so far.

In this communication, the PSD characteristics of CsI:Tl and GGAG:Ce,B scintillators are compared using two discrimination techniques based on charge integration and zero-crossing timing methods. In addition to the conventional photomultiplier tube, the PSD capabilities of SiPM based CsI:Tl and GGAG:Ce,B detectors were also evaluated.

* Corresponding author.

http://dx.doi.org/10.1016/j.nima.2016.09.060
Received 5 July 2016; Received in revised form 18 September 2016; Accepted 28 September 2016
Available online 29 September 2016
0168-9002/

2. Experimental details

Single crystals of GGAG:Ce,B were grown using the Czochralski technique. The concentration of “Ce” and “B” is 0.2 at% percent with respect to Gd in the initial charge for crystal growth. The codoping with boron was used based on our recent work on the improvement of scintillation performance [4]. The CsI:Tl crystals were grown using the Bridgman technique having 0.15 at% concentration of “Tl” in the initial charge. The growth processes for these crystals in details have been discussed in the recent publication [19]. Two samples of CsI:Tl and GGAG:Ce,B having similar dimensions of 18×18×10 mm^3 were cut from the grown crystals. The surface which was coupled to photosensors was optically polished while the other surfaces including the surface on which the source was mounted were used in an as-cut state from the grown crystal without any further treatment. The samples were coupled to 2″ Hamamatsu R1306 PMT using optical grease for an efficient light collection.

In another set of experiments, an optical guide was used to couple the crystals on SiPM (SenSL C type) having 6×6 mm^2 active area. The SiPM mounted on a PCB board having dual mode readout of fast and standard outputs was used in the zero-crossing method to get both timing and energy information from each pulse. It is operated at an overvoltage of 4 V (V_{br}~27.5 V). Overvoltage makes its photon detection efficiency to be 42%. The temperature of the laboratory was controlled and maintained at 25 °C with the help of air conditioners. The PSD was measured with Am-Pu alpha source having energies of 5.14 and 5.48 MeV while ^{60}Co was used as a gamma source. The alpha source was mounted on the crystal's non-polished surface. A 25 µm thick aluminum foil having 2 mm opening hole was used as a reflector and collimator between the source and crystal surface. The assembly was then tightly wrapped with Teflon tapes leaving minimum possible air gap in between. The gamma source was kept at a distance of 5 cm in front of the alpha-detector system. The PSD measurements were carried out by deploying charge integration and zero-crossing methods. A CAEN make 14 bit, 16 channels digitizer (V1730) with DPP-PSD firmware and a sampling rate of 500 MS/s was used to integrate the pulse and obtain the charges for the different short and long time gates associated with alpha particles and gamma rays. The integrated charge in short and long gates is computed by the digitizer due to different pulse shapes of alpha and gamma decay. The discrimination can be represented as a dimensionless parameter $PSD_{Digitizer}$ given by:

$$PSD_{Digitizer} = 1 - \frac{Q_S}{Q_L} \tag{1}$$

where, Q_S is the charge collected in the short gate due to prompt light emission while the total light (Q_L) is collected in the long gate. Various gate settings were used to observe the effect of charge collection on the discrimination and were subsequently optimized. The parameters such as charge sensitivity (80 fC), CFD fraction (75%), and pre-gate (130 ns) were also optimized to obtain the best possible discrimination. The optimum values for the threshold were 9.6 mV and 3.6 mV, and for the trigger hold-off were 1600 ns and 720 ns for CsI and GGAG crystals, respectively. A schematic diagram of the PSD measurement setup using the digitizer is shown in Fig. 1 using the gamma source.

In order to support the results obtained from the digitizer setup, a PSD technique for measuring zero-crossing time (ZCT) difference for

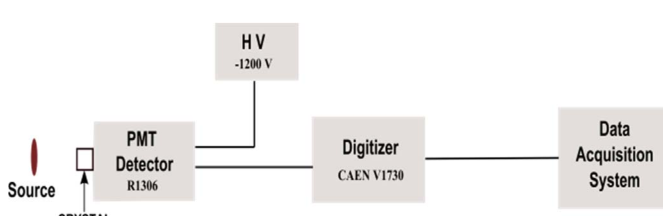

Fig. 1. A block diagram of PSD measurement setup using digitizer.

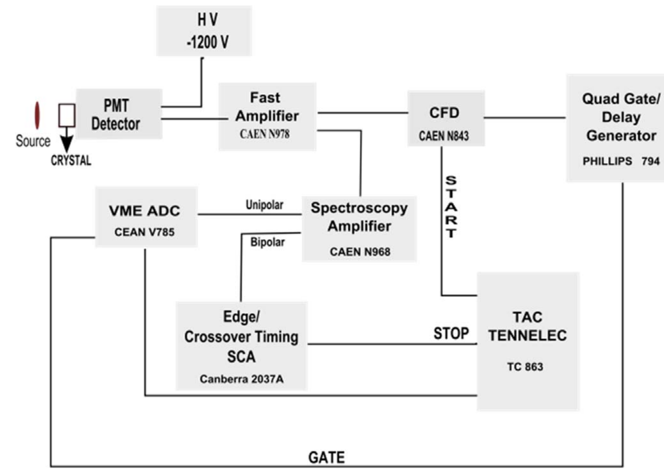

Fig. 2. A schematic diagram of PSD measurement setup using zero crossing time difference method.

gamma and alpha radiation was also used. Fig. 2 shows a typical ZCT setup using PMT as photo-sensor.

A similar setup was used for SiPM based detectors except an additional inverter. The detector pulses were then processed through a spectroscopy amplifier. The unipolar pulse from the amplifier was fed to a CAEN make VME analog-to-digital convertor (ADCV785) containing pulse height characteristics. While the other input of ADC through a time to amplitude (TAC) had the PSD parameter. Discrimination was achieved by measuring the ZCT of the amplified, bipolar pulse from the spectroscopy amplifier. However, a lower threshold cut-off was introduced to remove 59 keV gammas originating from the Am alpha source to obtain better FOM.

3. Results and discussion

The CsI:Tl and GGAG:Ce,B crystals grown by Bridgeman and Czochralski techniques respectively were found to be free from any visible cracks and inclusions. The processed samples of Tl doped CsI and B codoped GGAG:Ce single crystals having dimension of 18×18×10 mm^3 are shown in Fig. 3.

The samples were directly coupled to the PMT. However, a uniquely designed light-guide (Fig. 3) played a crucial role in coupling the larger samples with the SiPM for the maximum light collection. The light guide did not introduce any significant variation in the pulse height and the energy resolution was found comparable to that ~~of~~ measured for 5×5×5 mm^3 crystals that were directly coupled to the SiPM.

Fig. 4 shows the normalized scintillation decay plots of CsI:Tl and GGAG:Ce,B crystals measured directly from the anode of the PMT using a fast digital oscilloscope.

The relative ratio of component decay curves recorded for alpha as well as gamma source consists of two components and therefore could be fitted using the following equation:

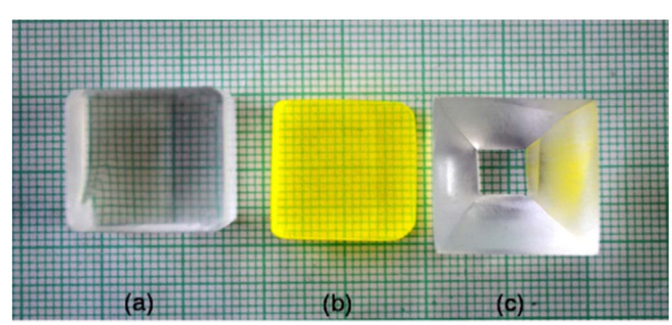

Fig. 3. Single crystal of (a) CsI:Tl and (b) GGAG:Ce,B and (c) a light guide for coupling crystals with SiPM.

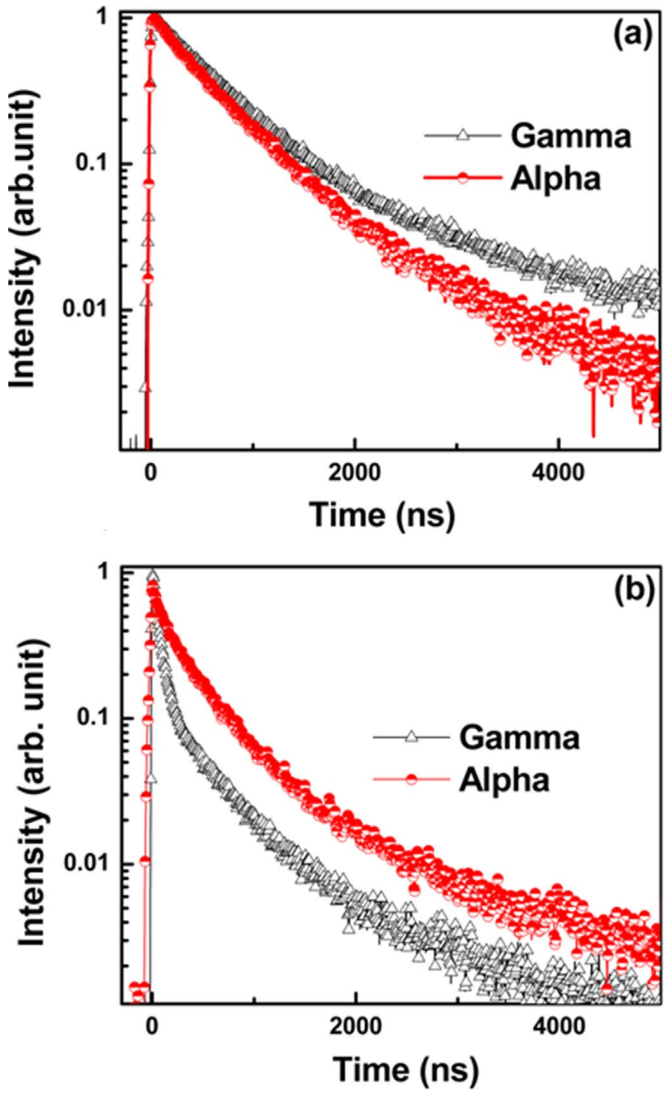

Fig. 4. Normalized scintillation decay curves measured with alpha and gamma sources for (a) CsI:Tl and (b) GGAG:Ce,B crystals coupled to PMT.

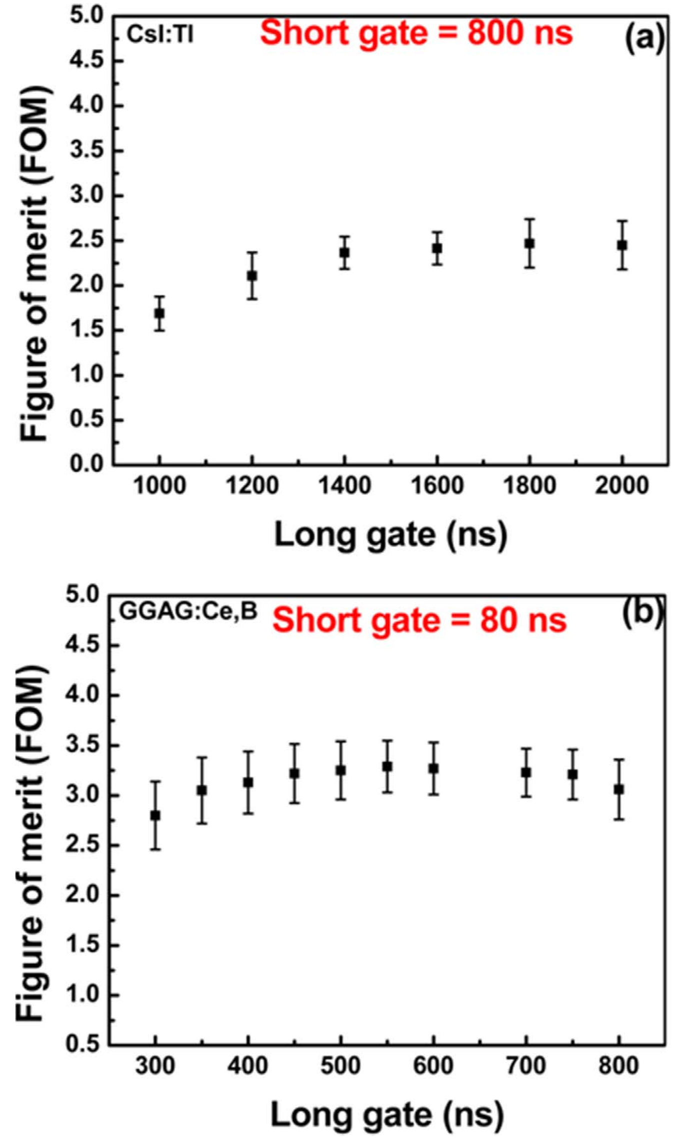

Fig. 5. The effect of long gate settings on figure of merit (FOM) measured for (a) CsI:Tl and (b) GGAG:Ce,B crystals coupled to PMT.

$$I(t)=A_0+A_1\exp(-t/\tau_1)+A_2\exp(-t/\tau_2) \quad (2)$$

The relative ratio of decay components was calculated from the equation:

$$Q_1=\frac{A_1\tau_1}{A_1\tau_1+A_2\tau_2} \quad (3)$$

and the average decay time was calculated from:

$$\tau=\frac{A_1\tau_1+A_2\tau_2}{A_1+A_2} \quad (4)$$

where, τ_1 and τ_2 denote the fast and slow decay time components respectively and A_1, A_2 denote their relative contributions in the total pulse intensity.

The decay time components of CsI:Tl detector for alpha excitation was measured to be 300 ns and 700 ns with relative intensities of 25% and 75% respectively. The corresponding average life time (amplitude weighted) was calculated to be about 600 ns. The decay time for gamma excitation is 700 ns and 3500 ns respectively with relative contributions of 57% and 43% respectively with gamma average decay time of 1200 ns. These values are in good agreement with those were reported earlier [20]. The acceleration of decay time due to alpha in comparison with gamma excitation may be attributed to the non-radiative quenching of the emission. Higher ionization density of alpha particles cause the interaction of excited Tl^{+} state with excited atoms which consequently leads to non-radiative quenching of the emission [21,22].

However, the excitation in GGAG:Ce,B does not seem to follow the similar relaxation mechanism. In these crystals the faster decay component at 61 ns and the slower one at 488 ns were found to have relative contributions of 77% and 23% respectively for gamma excitation. The fast component has been assigned to the transition from 5d-4f state in Ce^{3+} while the slow component arises due to the presence of defect centers [23]. The average life time of gamma excitation is 108 ns. While, in contrast to CsI:Tl, alpha radiation slows down the decay time having components of 104 ns and 501 ns with relative intensities of 20% and 80% respectively that led to the average time of about 284 ns. A similar mechanism has also been observed in an iso-structural YAG:Ce crystal [12]. Despite having a higher ionization density, there is an increase in the decay time for alpha excitation, which indicates the role of defect centers in the scintillation kinetics of these crystals. In order to understand the role of defects in relaxation mechanism of various excitation radiations, more experiments are in progress.

After observing the dependence of decay time on the ionization density, PSD studies of alpha particles and gamma rays were carried out by employing digitizer and zero-crossing setup. The PSD measure-

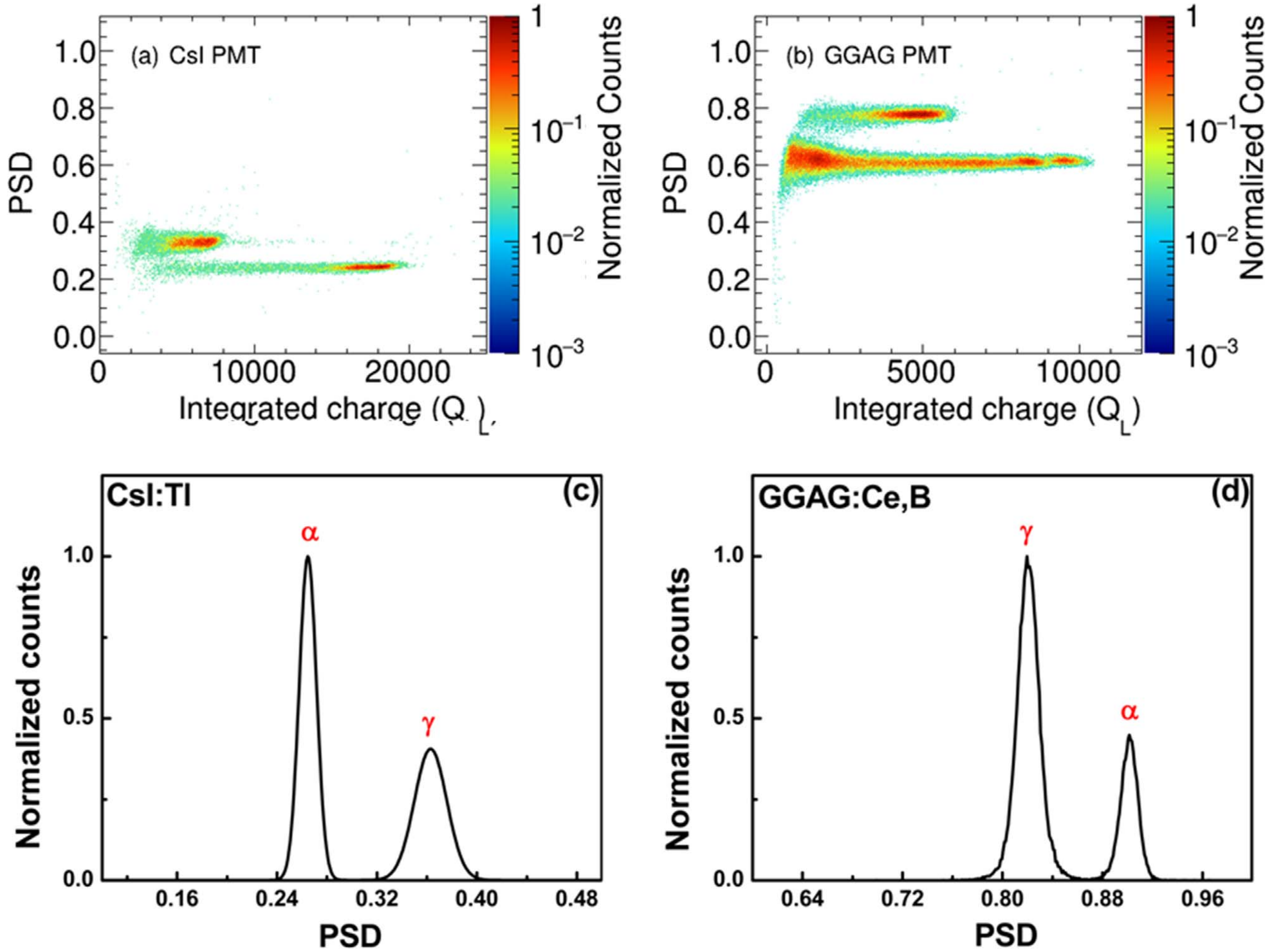

Fig. 6. Results of PSD measurement using digitizer for alpha and gamma rays of (a) CsI:Tl and (b) GGAG:Ce,B crystals coupled to PMT. The projection along X-axis is shown for (c) CsI:Tl and (d) GGAG:Ce, B.

ments, by using digitizer, are based on the charge collection in long (Q_L) and short gate (Q_S). The value of PSD, as given in Eq. (1), indicates the dependence of discrimination capability on Q_S/Q_L ratio. Therefore, to obtain the best PSD value, the corresponding gates are needed to be optimized for an effective capture of the fastest and the slowest components of light yield in short and long gates respectively. The excellence of figure of merit (FOM) describing the degree of discrimination between alpha and gamma pulses was calculated using:

$$FOM=\frac{\Delta T}{\tau_\alpha+\tau_\gamma} \tag{5}$$

where, ΔT is the separation between the centroids of two peaks in the TAC spectrum or PSD values from the digitizer. τ_α and τ_γ represent the FWHM of time or PSD gaussian distributions.

The effect of long gate selection on FOM, as shown in Fig. 5, indicates the importance of the relationship between charge collection through different gates and PSD. The short gate was optimized and fixed at 800 ns for CsI:Tl and 80 ns for GGAG:Ce,B. Initially, both graphs in the Fig. 5 depicted a trend of FOM getting better on increasing the long gate. However once a maximum is attained, the discrimination tends to either saturate or decrease. After measuring the FOM for various gate combinations, the short and long gates were optimized to 800 ns and 1600 ns respectively for CsI:Tl. Similarly, the values for short and long gates were optimized to 80 ns and 550 ns for GGAG:Ce,B respectively.

Fig. 6 [(a) and (b)] show the scattered plots of PSD as a function of the integrated charge for CsI:Tl and GGAG:Ce,B respectively. Its Y-axis represents the PSD values between 0 and 1, as calculated from Eq.(1), while the pulse height (energy) of alpha and gamma is plotted along the X-axis. Fig. 6 [(c) and (d)] are the projections of PSD for the entire energy range of alpha and gamma. The PSD scattered plot along Y-axis quantitatively states the degree of separation between alphas and gammas in terms of FOM.

The value of FOM depends on the separation and FWHM corresponding to Gaussian peaks of alpha and gamma. The α/γ light-yield ratio can be measured from the projection of the scattered graph along the X-axis. For CsI:Tl and GGAG:Ce,B crystals, the α/γ ratios were found to be 0.50 and 0.17 respectively. These values are reasonably in good agreement with the reported values [14,22]. Keeping in mind the resolution of the crystals, the mean energy of 5.14 and 5.48 MeV alpha particles was considered for the measurements.

The opposite dependence of the decay for alpha particles and gamma rays in CsI:Tl and GGAG:Ce,B can also be seen in Fig. 6. In CsI:Tl (Fig. 6a), the alpha excitation results in a faster decay time as represented by the lower blotch that appears at higher energies on X-axis owing to a relatively higher α/γ ratio. In the GGAG:Ce,B [Fig. 6(b)], the dependence is opposite where the spread on Y-axis represents alpha due to a longer decay time. The small α/γ ratio leads to the pulse height at lower channel numbers on the X-axis. Although a lower α/γ ratio for GGAG:Ce,B indicates stronger quenching due to high ionization density but it increases the decay time unlike CsI:Tl. The results point out the role of centers that release the trapped charges after some time and therefore increase in the decay time. The role of defect centers in scintillation kinetics has been explained by Tyagi et al. in Ref. [5]. In spite of having a poor α/γ ratio, there is a marked difference in the Y projection due to the pulse shape difference

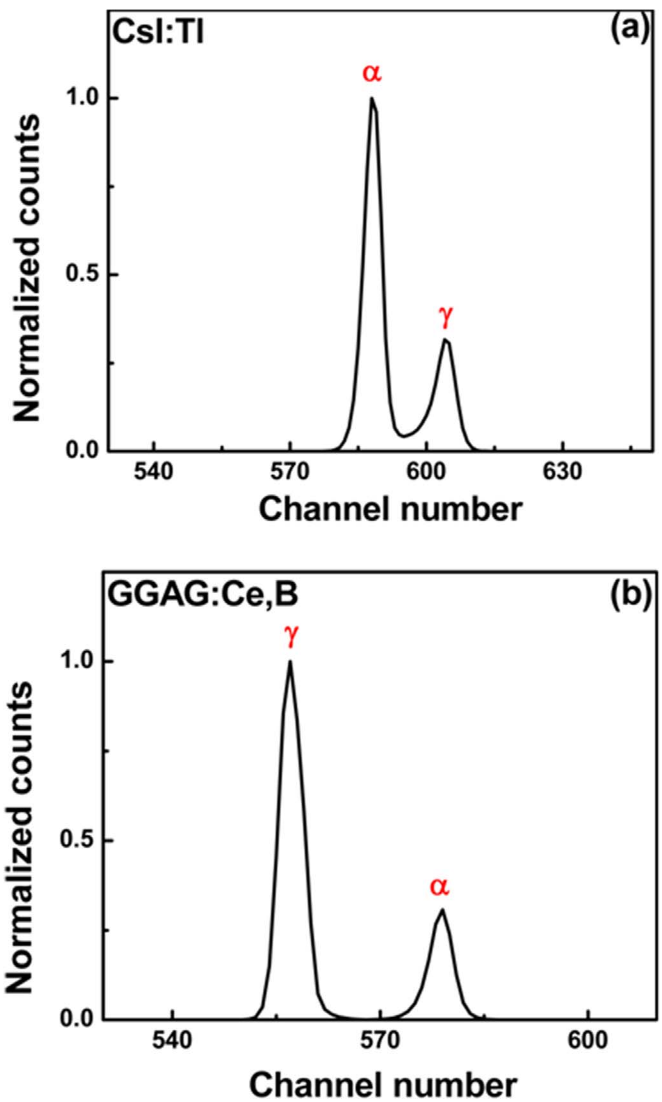

Fig. 7. PSD for alpha and gamma rays in (a) CsI:Tl and (b) GGAG:Ce,B crystals coupled to PMT from zero-crossing setup.

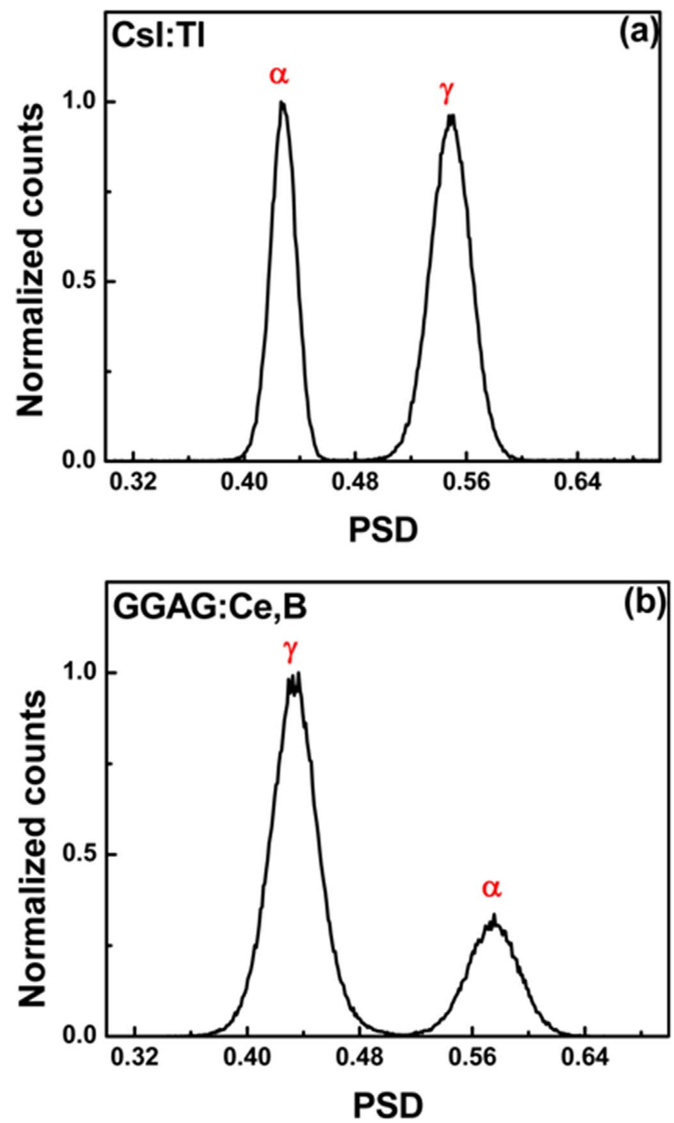

Fig. 8. PSD plots for alpha and gamma rays of (a) CsI:Tl and (b) GGAG:Ce,B crystals coupled to SiPM from Digitizer.

caused by alpha and gamma excitations in both the detectors. The FOM values for CsI:Tl and GGAG:Ce,B were calculated to be 2.41 and 3.42 respectively which illustrates the PSD capabilities of these detectors. Even though the α/γ ratio of CsI:Tl (0.50) is better than that of GGAG:Ce,B (0.17), FOM values suggest GGAG:Ce,B to be a better choice for the identification of charged particle based on the PSD. It may be noted that the results presented are for the energies greater than 122 keV.

Moreover, in order to corroborate the digitizer firmware results, zero-crossing time difference of both the detectors was also measured using the conventional zero-crossing method as shown in Fig. 7. The zero-crossing time difference of 89 ns and 60 ns for GGAG:Ce,B and CsI:Tl respectively was sensed by a Timing single channel analyzer (TSCA). The greater value of FOM for GGAG:Ce,B crystal supports the measured results obtained using the digitizer.

Exponential decay curves of both the crystals mounted on SiPM through light guide have also shown a similar dependence on alpha and gamma excitations as that measured with a PMT. The PSD comparison measured with the digitizer is shown in Fig. 8. The separation between alpha and gamma is quite apparent in both the detectors in a compact geometry employing SiPM. The measured zero-crossing time difference of 114 ns for a GGAG:Ce,B-SiPM detector was found to be better than 102 ns measured for the CsI:Tl-SiPM detector. These results support the results obtained by employing PMT. In SiPM based detectors, a higher PSD from the zero-crossing method suggests a better discrimination compared to PMT based detectors.

This may be attributed to better photon detection efficiency and a good matching between emission wavelength of the crystal and spectral sensitivity of the SiPM (550 nm). Better compatibility of GGAG:Ce scintillators with SiPM has already been reported by Tyagi et al. [18] in which they have demonstrated that the timing properties strongly depend on the digital processing system. However, the FOM for GGAG:Ce,B (1.54) is slightly less than that of CsI:Tl (1.71) which can be assigned to the energy spread especially at lower energies. It may be noted that SiPMs have a higher noise contribution due to their single photon sensitivity, crosstalk and after-pulsing. An improvement in the back-end electronics and data acquisition may result in a better FOM for the SiPM detectors in support of higher zero-crossing time.

4. Conclusion

In spite of a stronger quenching of emission, alpha excitation slows down the scintillation decay time in GGAG:Ce,B crystals unlike other halide scintillators where higher ionization density excitation makes scintillation decay faster. The PSD is observed to be better in

GGAG:Ce,B crystals in comparison to CsI:Tl. The FOM was calculated to be 3.4 in GGAG:Ce,B crystals which is higher compared to 2.4 in CsI:Tl crystals. The highest zero-crossing time difference of 114 ns was also obtained when GGAG:Ce,B scintillator was coupled with SiPM. However, lower FOM values from SiPM based detectors are expected to improve with better parameter optimization and electronics.

Acknowledgement

The authors would like to thank Dr. L.M. Pant NPD, BARC for his guidance and support.

References

[1] E. Mihkov, M. Nikl, J. Mare, et al., J. Lumin. 126 (2007) 77.
[2] K. Kamada, K. Tsutsumi, T. Endo, et al., Cryst. Growth Des. 11 (2011) 4484.
[3] J. Iwanowska, L. Swiderski, T. Szczesniak, et al., Nucl. Instrum. Methods Phys. Res. Sect. A 712 (2013) 34.
[4] M. Tyagi, A.K. Singh, S.G. Singh, et al., Phys. Status Solidi (RRL)- Rapid Res. Lett. 9 (2015) 550.
[5] M. Tyagi, F. Meng, M. Koschan, et al., J. Phys. D 46 (2013) 475302.
[6] Y. Tamagawa, Y. Inukai, I. Ogawa, M. Kobayashi, Nucl. Instrum. Methods Phys. Res. Sect. A 795 (2015) 192.
[7] C.M. Bartle, Nucl. Instrum. Methods Phys. Res. 124 (1975) 547.
[8] R.A. Winyard, J.E. Lutkin, G.H. McBeth, Nucl. Instrum. Methods 95 (1971) 141.
[9] E. Dafni, Nucl. Instrum. Methods Phys. Res. Sect. A 254 (1987) 54.
[10] T.L. White, W.H. Miller, Nucl. Instrum. Methods Phys. Res. A 422 (1999) 144.
[11] F. Crespi, F. Camera, N. Blasi, et al., Nucl. Instrum. Methods Phys. Res. A 602 (2009) 520.
[12] T. Ludziejewski, M. Moszynski, M. Kapusta, et al., Nucl. Instrum. Methods Phys. Res. Sect. A 398 (1997) 287.
[13] K. Kamada, T. Yanagida, J. Prjchal, et al., J. Cryst. Growth 352 (2012) 35.
[14] M. Kobayashi, Y. Tamagawa, S. Tomita, et al., Nucl. Instrum. Methods Phys. Res. Sect. A 694 (2012) 91.
[15] M. Alderighi, A. Anzalone, R. Basssini, et al., Nucl. Instrum. Methods Phys. Res. Sect. A 489 (2002) 257.
[16] D.L. Horrocks, Applications of Liquid Scintillation Counting, Academic Press Inc. (London) Ltd, London, 1974.
[17] A. Wagner, W.P. Tan, K. Chalut, et al., Nucl. Instrum. Methods Phys. Res. Sect. A 456 (2001) 290.
[18] M. Tyagi, V.V. Desai, A.K. Singh, et al., Phys. Status Solidi (a) 212 (2015) 2213.
[19] S.G. Singh, D.G. Desai, A.K. Singh, et al., J. Cryst. Growth 351 (2012) 88.
[20] J.D. Valentine, W.W. Moses, S.E. Derenzo, et al., Nucl. Instrum. Methods Phys. Res. Sect. A 325 (1993) 147.
[21] A.M. Kudin, E.P. Sysoeva, E.V. Sysoeva, Larisa N. Trefilova, D.I. Zosim, Nucl. Instrum. Methods Phys. Res. Sect. A 537 (2005) 105.
[22] L.E. Dinca, P. Dorenbos, J.T.M. de Haas, V.R. Bom, C.W.E. Van Eijik, Nucl. Instrum. Methods Phys. Res. Sect. A 486 (2002) 93.
[23] Mohit Tyagi, Harold Rothfuss, Samuel B. Donnald, Merry Koschan, Charles L. Melcher, IEEE Trans. Nucl. Sci. 61 (2014) 297.